# Nature of the Lewis Acid Sites on Molybdenum and Ruthenium Sulfides: An Electrostatic Potential Study

**Yosslen Aray,*,† Jesús Rodríguez,† Santiago Coll,† Eloy Nouel Rodríguez-Arias,§ and David Vega‡**

*Centro de Química, IVIC, Apartado 21827, Caracas 1020 A, Venezuela, FACYT, Universidad de Carabobo, Valencia, Venezuela, and Laboratorio de Modelaje de Catálisis, Departamento de Química, Universidad Simón Bolívar, Caracas, Venezuela*

*Received: July 25, 2005; In Final Form: October 11, 2005*

The energy of formation and the Lewis acid strength of sulfur vacancies or coordinative unsaturated sites on the $MoS_2$ edges were studied using density functional theory for periodic systems and an electrostatic potential-based methodology. The results suggest that the more energetically favorable sites are located on the sulfur edges; however, their Lewis acid strength is considerably smaller than the site acidity at the molybdenum edges. The acid strength for the reported most hydrodesulfurization active site of $RuS_2$ was also determined. In general, the Lewis acid for the site on $RuS_2$ is 100% smaller than the sites on the Mo edges and around 20% larger than the most favorable site on the S edges of $MoS_2$. Binding of the pyridine molecule in the $\eta_1$ adsorption configuration on the considered sites has corroborated the trend of Lewis acidity suggested by the electrostatic potential methodology.

## Introduction

Transition-metal sulfides (TMSs) belong to a very important class of catalysts characterized by being stable under strong conditions in hydrodesulfurization (HDS), hydrodenitrogenation (HDN), and hydrogenation reactions.[1,3] In these processes, the surfaces of the sulfides are reduced by sulfur elimination using a large excess of hydrogen at temperatures ranging from 573 to 673 K creating coordinatively unsaturated sites (CUSs) or vacancies around the metals. A CUS intervenes as an electron-withdrawing site whose properties may be regarded as a Lewis-type center interacting with electrodonating organic substrates.[4−6] The nature of these sites is suggested to be intimately related to the metal−sulfur bond strength.[4,5,7,8] Basic studies support the view that differences in catalytic activities are related to variations in the concentration of CUSs (the Lewis acid sites), which in turn depend on the metal−sulfur bond strength.[9−20] Molybdenum-based catalysts have for many years been among the most important catalysts in the refinery service. However, $RuS_2$ is one of the most active TMSs, being a promising candidate to replace $MoS_2$-based catalysts to meet new and more stringent refinery requirements. Studies using X-ray absorption fine structure (EXAFS) have established that the active Mo atom is present as small $MoS_2$-like nanostructures.[21,22] Adsorption and activity experiments[23,24] have revealed that the active sites reside at the edges of the $MoS_2$ structures, and recently, high-resolution scanning tunneling microscopy (STM) and density-functional theory (DFT) studies[25] have shown that the $MoS_2$ nanoclusters adopt a hexagonal shape exposing two different types of edges: Mo edges covered with S monomers and fully sulfur-saturated S edges with H atoms adsorbed (i.e., S−H groups). Similar studies on $RuS_2$ nanoclusters using STM[26] and theoretical calculations[27,28] on periodic surfaces have suggested that the (111) plane is responsible for the $RuS_2$ catalytic activity. The STM studies have demonstrated the formation on the Au-(111) substrate of hexagonal flat $RuS_2$ islands with an area of 30 $nm^2$. Unlike the situation for the $MoS_2$ nanoclusters, a high density of sulfur vacancy is present on the flat (111) surface of the $RuS_2$ nanostructures. To continue improving the understanding of HDS catalysts, in the present article, we explore the nature of the acidic sites on these $MoS_2$ and $RuS_2$ nanostructures using an ab initio electrostatic potential methodology.

## Theory and Computational Methodology

The nature of active sites can be particularly explored using the electrostatic potential $V(\mathbf{r})$, which lets us directly determine where the electron-rich sites in a molecule or crystal are localized.[29−39] $V(\mathbf{r})$ at a point $\mathbf{r}$ generated by a molecule or crystal is given by

$$V(\mathbf{r}) = V_N(\mathbf{r}) + V_E(\mathbf{r}) \tag{1}$$

where the two terms $V_N(\mathbf{r})$ and $V_E(\mathbf{r})$ represent the bare nuclear and electronic contributions, respectively, to the total electrostatic potential. The sign of $V(\mathbf{r})$ at a given point indicates whether the nuclear (positive) or electronic (negative) effects are dominant. The electrostatic potential at $\mathbf{r}$ generated by the total charge distribution $\rho^{tot}$ of a periodic system is given by

$$V(\mathbf{r}) = \sum_n \int \rho^{tot}(\mathbf{r}' - \mathbf{R}_n)|\mathbf{r} - \mathbf{r}'|^{-1}\, d\mathbf{r}' \tag{2}$$

The summation extends to all direct lattice vectors, the prime on the integral sign indicating that an infinitesimal region about $\mathbf{r} = \mathbf{r}'$ is excluded from the domain of integration to avoid divergent nuclear self-interaction terms that would otherwise arise in the electrostatic energy per cell. $\rho^{tot}$ may be decomposed

* To whom correspondence should be addressed. E-mail: yaray@ivic.ve. Fax: 58-2-504-1336.
† IVIC.
‡ Universidad de Carabobo.
§ Universidad Simón Bolívar.

10.1021/jp054097t CCC: $30.25 
Published on Web 11/17/2005

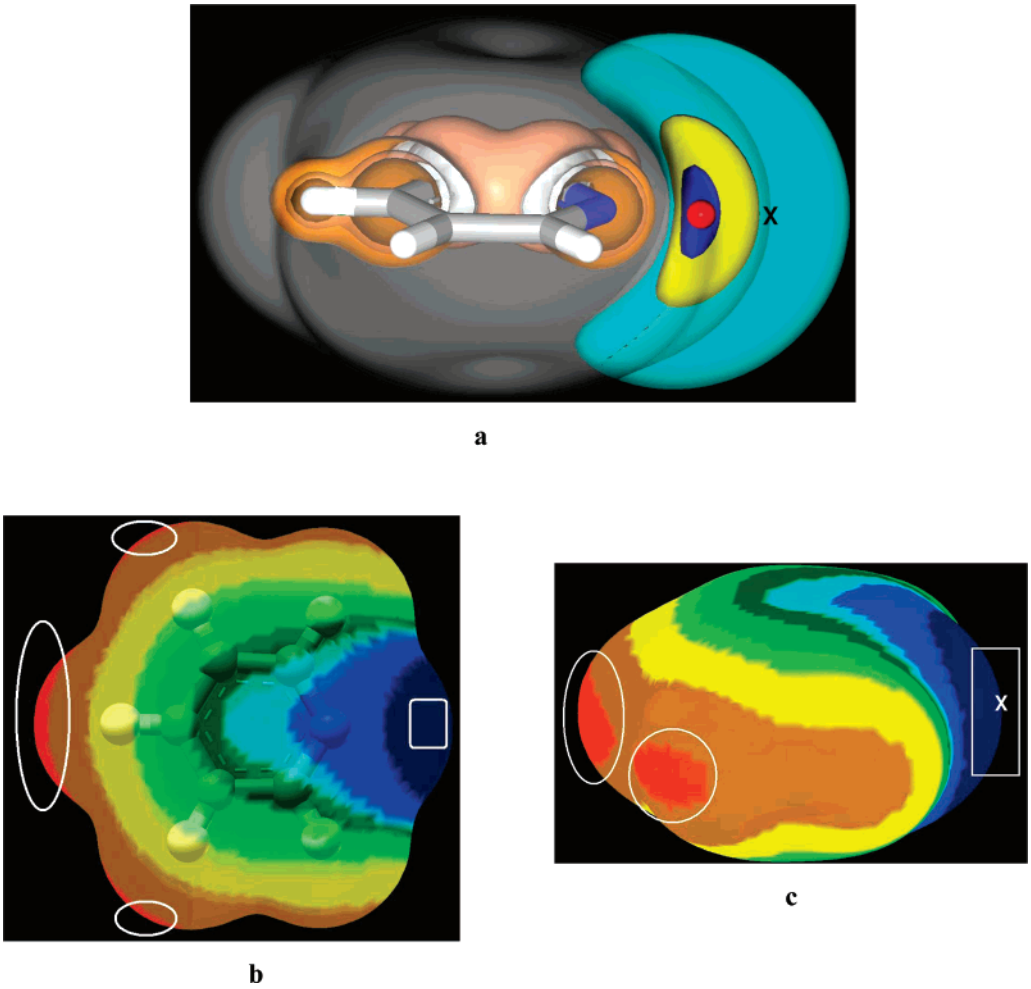


**Figure 1.** (a) Side view of a cylinder model representation and some $V(\mathbf{r})$ contours for the pyridine molecule. Blue, gray, and white cylinders denote the N, C, and H atoms, respectively. Blue, yellow, and light-blue isosurfaces denote negative $V(\mathbf{r})$ zones with values of −210.040, −131.275, and −52.510 kJ/mol, respectively. Brown isosurfaces denote positive $V(\mathbf{r})$ zones. The gray isosurface denotes the 0.002 au contour of $\rho(\mathbf{r})$, which is used to reveal the sites most susceptible to electrophilic attack. (b) Top and (c) side views of the 0.002 au contour of $\rho(\mathbf{r})$ mapping the $V(\mathbf{r})$ field values onto colors. The color map tabs are blue jay (−157.530 to −78.765 kJ/mol), blue heaven (−78.765 to 42.008 kJ/mol), light blue (−42.008 to −31.506 kJ/mol), dark green (−31.506 to −21.004 kJ/mol), green (−21.004 to −10.502 kJ/mol), light green (−10.502 to 0.000 kJ/mol), yellow (0.000 to 26.255 kJ/mol), cream yellow (26.255 to 52.510 kJ/mol), orange (52.510 to 65.638 kJ/mol), brown (65.638 to 78.765kJ/mol), purple (78.765 to 91.893 kJ/mol), light red (91.893 to 105.020 kJ/mol), and red (105.020 to 144.403 kJ/mol). The white square and ellipsoids indicate the most negative and positive zones on the $\rho(\mathbf{r})$ contour, respectively. An X denotes the $V(\mathbf{r})$ minimum point on the $\rho(\mathbf{r})$ isosurface.

into electronic and nuclear components

$$\rho^{\text{nuc}}(\mathbf{r}) = \sum_a q_a \delta(\mathbf{r}_a, \mathbf{r}) \tag{3}$$

where the summation extends to all of the reference cell nuclei, with atomic numbers and position vectors denoted $q_a$ and $\mathbf{r}_a$, respectively.

$$\rho^{\text{el}}(\mathbf{r}) = -\sum_{ij}\sum_{\mu\nu} \mathbf{P}_{\mu\mathbf{R}_i\nu\mathbf{R}_j} \chi_\mu(\mathbf{r} - \mathbf{R}_i)\chi_\nu^*(\mathbf{r} - \mathbf{R}_i) \tag{4}$$

where $\mathbf{P}$ is the density matrix and $\chi_\mu(\mathbf{r} - \mathbf{R}_i)$ is the $\mu_{th}$ reference cell basis function translated by the direct lattice vector $\mathbf{R}_i$. The summations over $i$ and $j$ extend to all direct lattice vectors, whereas those over $\mu$ and $\nu$ include all of the basis functions of the reference cell. Substituting eqs 3 and 4 into eq 2 gives the nuclear and electronic $V(\mathbf{r})$ contributions.

For the region closest to the nucleus, $V_N$ dominates, and $V(\mathbf{r})$ has similar topology to that of the electron density[40,41] $\rho(r)$; that is, positive-valued maxima at the nuclear site and a positive-valued saddle point between every pair of bonded atoms. Nevertheless, the existence of maxima is ruled out via an established result that, barring the nuclear position, there cannot exist any strict local maxima in the $V(\mathbf{r})$ map.[32,33] For the region where $V_E$ dominates ($V(\mathbf{r})$ is negative), the $V(\mathbf{r})$ topography can be more complex. However, it is well known that lone pairs of electrons as well as double $\pi$ bonds (C═C, C═N, etc.) are generally characterized as negative-valued minima.[31,33] In summary, the region closest to the nucleus is always positive-valued, and the region where the potential is negative-valued contains the minima that characterize the atom lone pairs. The main topographic features of $V(\mathbf{r})$ are easily visualized using 3D maps of isovalued contours. For example, Figure 1a shows the $V(\mathbf{r})$ topological features of an isolated pyridine molecule PY, with the negative potential (blue, yellow, and green isosurfaces) located over the nonbonding region (above and below the molecular plane) of the rings, and of the N atom forming a lone pair pattern for the N atom with one negative-valued minimum (red sphere), whereas $V(\mathbf{r})$ over the entire nuclear region is just positive (brown zone). The minima of the negative region denote the zones to which an approaching electrophile may be attracted. On the contrary, the positive regions do not have maxima that might indicate sites for nucleophilic attack. Nevertheless, Politzer and Sjoberg have

shown that by computing $V(\mathbf{r})$ on the 0.002 e/bohr$^3$ contour isosurface[42] of the molecular electronic density $\rho(\mathbf{r})$ we can quantify the susceptibility of molecules to nucleophilic attack. They demonstrated that relative magnitudes of the positive electrostatic potential in various regions on this surface reveal the sites most susceptible to nucleophilic attack. This contour isosurface for a group of diatomic molecules and methane encompasses at least 95% of the electronic charge and yields physically reasonable molecular dimensions.[42] In the present work, we have used a similar approach, mapping on this isosurface the $V(\mathbf{r})$ values onto colors to identify the host sites onto which nucleophiles (most negative zone) and electrophiles (most positive zone) should bind. Additionally, to quantify the active sites' susceptibility we have also determined the minimum and maximum $V(\mathbf{r})$ values at these determined host zones using a Newton−Raphson technique developed in our laboratory, such as those that we have previously reported for the study of the electronic density[43] and electrostatic potential topology.[38,39,44] For example, this $\rho(\mathbf{r})$ contour for PY, in Figure 1a, is also shown as a gray isosurface, whereas Figure 1b and c shows a side and a top view of the corresponding mapping, respectively. The negative zone embraces the nonbonding region of the N atom (blue zone) and the ring (green zone), above and below the molecular plane with a minimum value (X symbol in Figure 1a and 1c) of −115.522 au located just on the molecular plane and at the right end of the dark-blue zone. Maintaining complementarity between the $V(\mathbf{r})$ features of the catalyst's surface and molecules, this minimum site of PY should be positioned over the maximum positive $V(\mathbf{r})$ zone on the catalyst's surface.

$V(\boldsymbol{r})$ was calculated by means of the Dmol$^3$ [45,46] program using the Kohn−Sham Hamiltonian with the gradient-corrected Perdew−Becke−Ernzerhof (PBE) exchange-correlation functional.[47] Dmol$^3$ calculates variational self-consistent solutions to the DFT equations expressed in an accurate numerical atomic orbital basis. The solutions to these equations provide the molecular electron densities, which can be used to evaluate the total electrostatic potential of the system. The numerical double-$\zeta$-plus polarization basis set DNP[45,46] was used in all calculations. DMol$^3$ uses DFT to obtain high accuracy while keeping the computational cost fairly low for an ab initio method.

## Catalyst Models

STM allows direct imaging of the catalytically relevant surface structure on the atomic scale. By studying[25] a realistic HDS model system consisting of a few-nanometers-wide gold-supported $MoS_2$ particles, it was shown that the morphology of the nanoparticles is sensitive to sulfiding and reactions conditions, that is, triangles under heavy sulfiding conditions or truncated hexagons under more sulfo-reductive conditions resembling HDS conditions. These hexagonal clusters expose the basal plane and two different types of edges: Mo edges covered with S monomers and fully saturated S edges with H atoms adsorbed.[25] Different models have been used to study the edge structure of $MoS_2$ catalysts using DFT methods: cluster models including a finite number of atoms,[48,49] a single S−Mo−S periodic slab,[50,51] and a larger slab model containing two S−Mo−S sheets exposing Mo and S edges alternatively.[18,52−61] From these studies, a clear picture of the $MoS_2$ edge structure has emerged. The most external Mo atoms of the Mo edge contain 50% sulfur coverage with each sulfur atom bridged to two neighboring molybdenum atoms. A significant reconstruction of the Mo edge takes place: the bridged S atoms are shifted by half a lattice constant relative to the bulk S lattice,

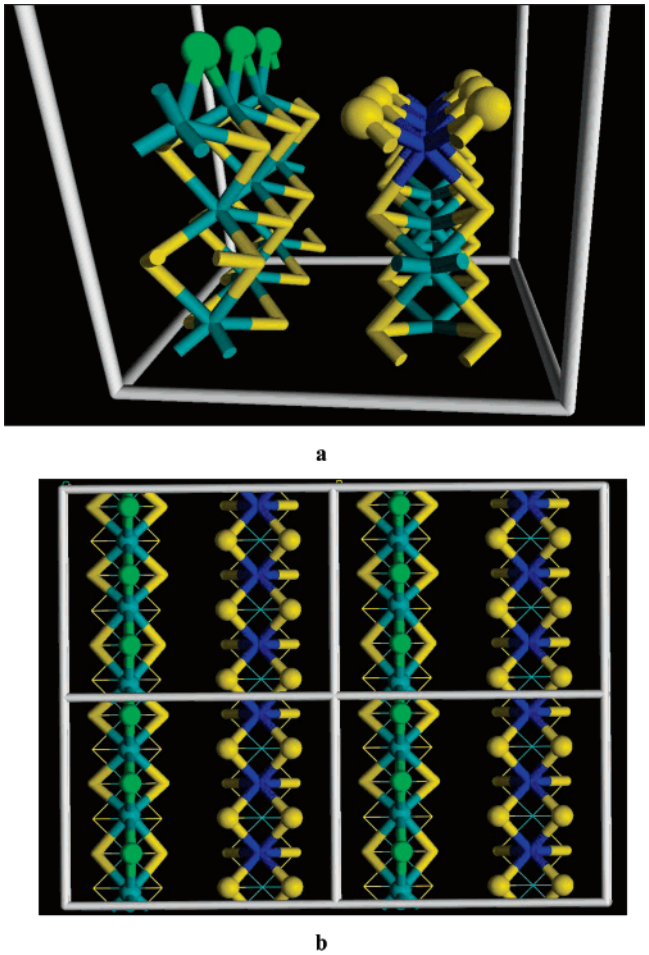

**Figure 2.** (a) Side view of the unit cell and (b) top view of a 2 × 2 supercell of the periodic model of the $MoS_2$ edges. Light-blue and yellow cylinders denote the Mo and S atoms, respectively. Dark-blue cylinders denote the Mo atoms on the S edges. Green and yellow spheres denote the outermost S atoms on the Mo and S edges, respectively.

and they move down to a bridging position in plane with the Mo lattice. The S edges remain fully sulfide, and a maximum Mo coordination to six sulfur atoms is achieved in one configuration where the edge is terminated by a row of sulfur atoms positioned in the bridge position close to those expected from bulk-terminated $MoS_2$. Both edge geometries lead to a coordination number of six for the outermost molybdenum atoms and two for the corresponding sulfur atoms. We have modeled the edge sites by means of the larger slab model (Figure 2) that exposes alternating layers of Mo and S edges denoting nanoparticles several layers wide. The unit cell (9.480 × 12.294 × 36.000 Å$^3$) of this surface exhibits three- and six-bridged S atoms on the Mo and S edges, respectively.

STM studies[26] of ruthenium sulfide synthesized on an Au-(111) surface have demonstrated the formation of a flat $RuS_2$ nanoisland with a higher density of sulfur vacancies than that for $MoS_2$, located on the flat $RuS_2$ surface with a periodicity of 0.8 nm aligned along the Au lattice. The flat islands have been shown as $RuS_2$ nanocrystals with the (111) plane parallel to the Au(111) substrate. Figure 3a shows an ideal model of such nanoclusters. In this Figure, the white circles denote the sulfur vacancies. We have modeled this flat surface using a periodic lattice (Figure 3b) containing sulfur vacancies as previously reported.[28] The $RuS_2$ bulk is a pyrite-type crystal whose lattice[62] is described by the cubic space group $Pa3$ with cube edge length $a = 5.611$ Å. Its structure can be described as a face-centered

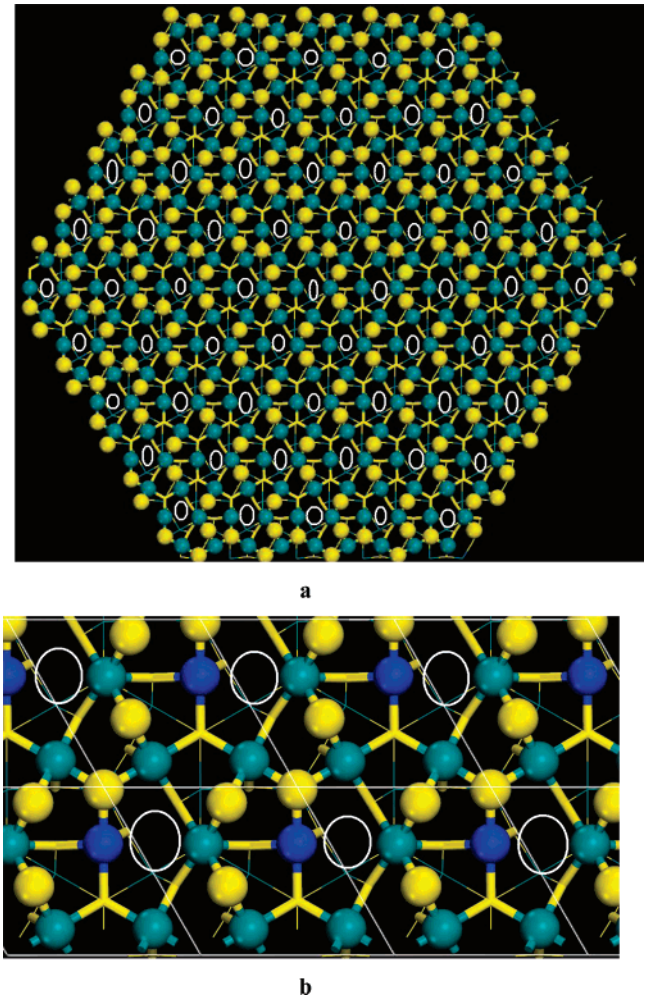

**Figure 3.** (a) Ball and cylinder model showing the top view of a hypothetical $RuS_2$ nanoparticle that simulates the nanoislands of ref 26. Blue and yellow spheres denote the Ru and S atoms, respectively. White circles denote the hollow site produced by the outermost sulfur vacancies. (b) Top view of the periodic surface used to model the nanoparticle sites showing the hollow site formed by three five-coordinate Ru atoms and one four-coordinate (dark-blue balls) Ru atom.

cube of Ru atoms with pairs of $S_2$ molecules located in the middle of the cube edges and at the cube center.[28] The (111) surface has a hexagonal unit cell whose vectors lie along the diagonals of the cube faces. This unit cell contains four Ru atoms per layer and eight S atoms above the Ru plane forming four $S_2$ pairs.[27,28] Three pairs are tilted on the surface, whereas the remaining one is oriented perpendicular to the surface with one S atom three-coordinate to the closest Ru plane and its topmost sulfur not directly bonded to ruthenium. The S atoms form four layers with slightly different heights on each side of a Ru layer. Thus, there are four S layers between two consecutive Ru layers. Similar to the bulk case, all of the Ru atoms of this surface are six-coordinate. The stoichiometric surface[27,28] is obtained by removing the two outermost S layers (top atoms of the $S_2$ layers). Then, all of the top S atoms correspond to broken $S_2$ pairs. On the furthest S layer there are three S atoms in the unit cell, each one sitting on a Ru bridging site, whereas there is only one on the next S layer, which is located on a three-fold Ru site. The topmost Ru plane of this surface contains six- and five-coordinate atoms. The active surface[27,28] is produced by a further reduction of one bridging sulfur atom per unit cell leading to a hollow site (denoted as white circles in Figure 3b) formed by three five-coordinate ruthenium atoms and one four-coordinate Ru atom (denoted as dark-blue spheres in Figure 3b).

The chosen systems were modeled by cells containing a periodic slab of several layers of atoms initially having the same structure of the surface built directly from the bulk. Vacuum layers thicker than 15 Å were used to ensure that there were no interactions between adjacent slabs. The geometry of those models was optimized using algorithms included in the Dmol$^3$ program.[45,46] The two upper rows were allowed to relax, whereas the atoms of the lower ones were kept fixed at their optimized bulk positions to simulate bulk constrains. Eight $k$ points were used to integrate the wave function in reciprocal space.

## Results and Discussion

The colors maps are made of 13 items (Figure 4 and the caption of Figure 1): 6 and 7 ranges in the negative and positive $V(\mathbf{r})$ values, respectively. Starting from the most negative values, there are three kinds of blue, three kinds of green, two yellows, one orange, one brown, one purple, and two kinds of red. The most negative and positive zones on these maps are highlighted by means of white spheroids and squares, respectively. In general, there is a minimum $V(\mathbf{r})$ value just in the middle of each square and a maximum inside each spheroid. Figure 4a shows a side view of the 0.002 e/bohr$^3$ contour of $\rho(\mathbf{r})$ for the periodic model of the most stable structure of the $MoS_2$ edge sites (site 1), whereas Figure 4b shows a top view of the $V(\mathbf{r})$ mapping onto colors. One may appreciate that the entire surface is colored with negative values (blues and greens) with a minimum value of $-49.622$ kJ/mol located just in the middle of every pair of the nearest sulfur atoms on the S edge. Accordingly, this $V(\mathbf{r})$ mapping shows that this surface mainly involves repulsive interaction with the negative minimum on nitrogen or sulfur atoms of molecules such as pyridine or thiophene. This result agrees with the known inactivity of this kind of site, such as basal plane, that exposes only sulfur atoms. Therefore, we have to create vacancies or CUSs on this surface by a reduction process to generate available Lewis acid sites. Usually $H_2$ reacts with surface sulfur atoms to create a vacancy and produce $H_2S$; therefore, the energy to create a sulfur vacancy can be calculated using the following equilibrium: surface-S $+ H_2 \leftrightarrow$ surface-□ $+ H_2S$. Thus, the creation energy, CE, of a sulfur vacancy is given by the expression

$$\mathrm{CE} = E(\text{Surface-}\square) + E(H_2S) - E(\text{Surface-S}) - E(H_2) \quad (5)$$

The energy of each sulfur removal has been reported, and the stability of each surface has been deduced using DFT methodology based on pseudopotentials and plane wave basis sets.[62] On the sulfur edge, we have studied the gradual removal of the six S atoms of the unit cell, and for each case, the geometrical optimization of the reported most stable configuration was carried out. Removing just one S atom of the S edge leads to a surface containing negative $V(\mathbf{r})$ values that are similar to those of site 1 involving repulsive interaction with the PY molecule. The remaining S atom on the vacancy moves to a bridging position in plane with the Mo atoms similar to the outermost S atoms on the Mo edges. Therefore, to obtain an appreciable Lewis acidity, at least two sulfur atoms have to be removed from the S edges. For the Mo edge, we have studied the gradual removal of the three S atoms ending with the full exposure of the underlying Mo atoms. The CEs (eq 5) of the studied sites are listed in Table 1, and the corresponding $V(\mathbf{r})$ mappings are shown in Figures 4c−i. Additionally, the $V(\mathbf{r})$ maximum values that characterize the site's Lewis acid strength are also reported in Table 1.

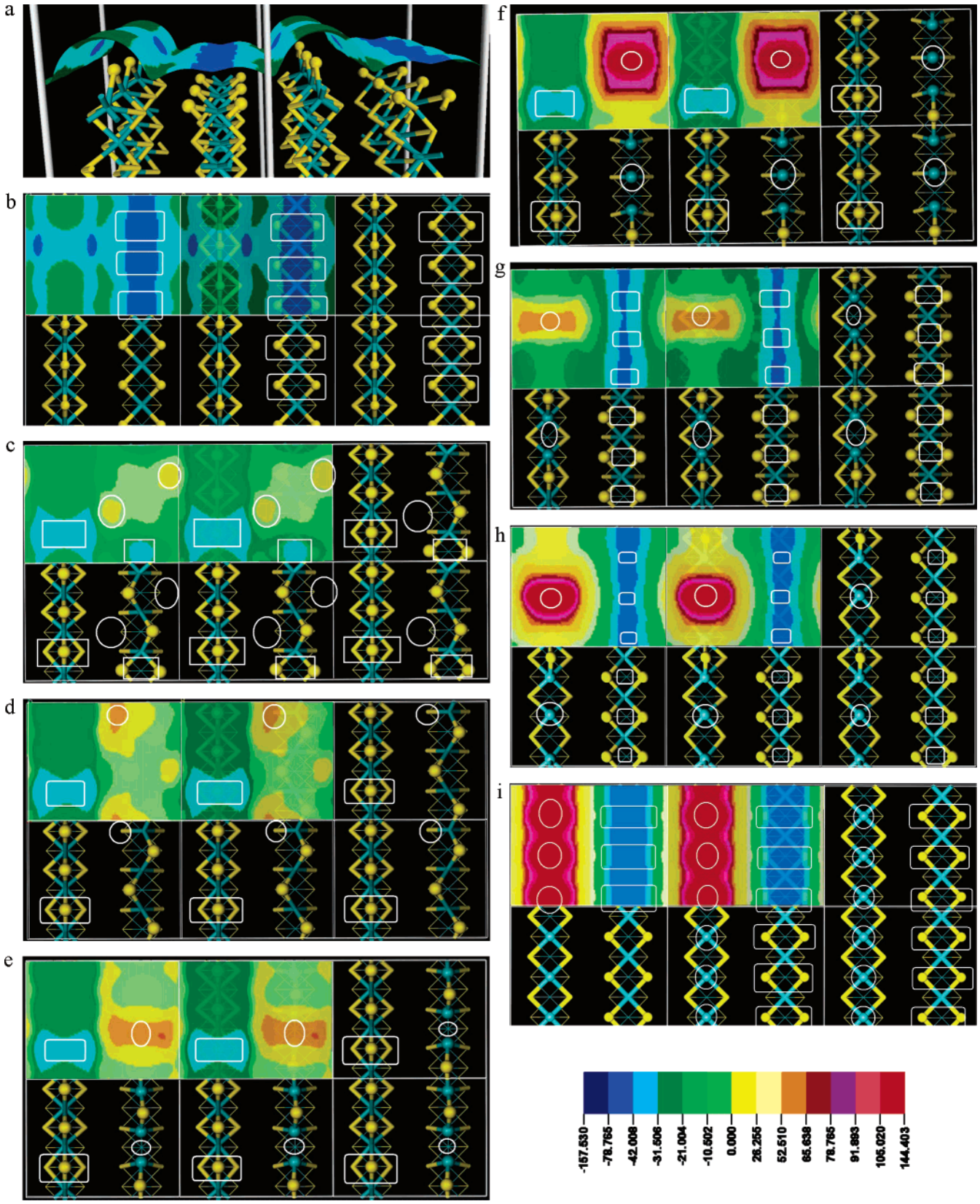


**Figure 4.** Top (a) and side (b) views of the 0.002 au contour of $\rho(\mathbf{r})$ showing the mapping of the $V(\mathbf{r})$ values onto colors for site 1 and the corresponding top views for sites 2 (c), 3 (d), 4 (e), 5 (f), 6 (g), 7 (h), and 8 (i). At the bottom, the color map tab is shown in kJ/mol. White squares and ellipsoids indicate the most negative and positive $V(\mathbf{r})$ zones, respectively. Blue and yellow cylinders denote the Mo and S atoms, respectively. Spheres denote the outermost and exposed atoms of the edges.

Site 2 (Figure 4c) exhibits five- and four-coordinate (distorted tetrahedron) Mo atoms on the S edge. For this site, small areas of yellow zones localized at both sides of the four-coordinate Mo atoms with a maximum of 15.491 kJ/mol can be observed. Removing an additional S atom (site 3) produces a site with three outermost four-coordinate Mo atoms by the unit cell. Two of these atoms have distorted tetrahedral geometry, whereas the other has a perfect tetrahedral arrangement (Figure 4d). The

**TABLE 1: Creation Energy, CE[a], and Maximum Positive Value of $V(\mathbf{r})$ for the Studied Sites on the Mo and S Edges of Molybdenum Sulfide**

| site | edge | number of sulfur atoms removed | CE (kJ/mol) | $V(\mathbf{r})$ maximum (kJ/mol) |
|---|---|---|---|---|
| 2 (Figure 4c) | S | 2 | 34.581 | 15.491 |
| 3 (Figure 4d) | S | 3 | 72.579 | 51.982 |
| 4 (Figure 4e) | S | 4 | 260.579 | 54.085 |
| 5 (Figure 4f) | S | 5 | 515.409 | 131.695 |
| 6 (Figure 4g) | Mo | 1 | 153.345 | 44.371 |
| 7 (Figure 4h) | Mo | 2 | 271.810 | 142.040 |
| 8 (Figure 4i) | Mo | 3 | 458.538 | 142.877 |

[a] Equation 5.

mapping of Figure 4d shows a cream-yellow zone on the left side of the perfect tetrahedron with a maximum of 51.982 kJ/mol. This corresponds to a 3-fold increase in the Lewis acidity with respect to that of site 2, whereas the energy cost for creating such a site is two times bigger than that of site 2. Site 4 is created by removing an additional S atom from site 3 and exhibits (Figure 4e) one four-coordinate and two three-coordinate outermost Mo atoms with tetrahedral and trigonal pyramid geometries, respectively. This site (Figure 4e) shows a cream-yellow zone with a positive maximum of 54.085 kJ/mol just above the middle of the trigonal Mo atoms. This $V(\mathbf{r})$ value suggests a Lewis acid strength that is almost the same as that of site 3, but it requires around 400% more energy than site 3 does to be created. Finally, site 5 is obtained by removing an additional S atom from site 4, and it exposes (Figure 4f) one two-coordinate and two three-coordinate Mo atoms by the unit cell with angular and trigonal pyramid geometries, respectively. A high-valued positive zone colored in red with a maximum of 131.695 kJ/mol, just above the angular Mo atom, can be observed. This means a large increment in the site Lewis acidity but at the cost of a huge CE as we can see in Table 1. Thus, sites 4 and 5 are very energetically unfavorable with respect to the other S-edge sites. Site 2 is most easily created. However, the small positive zones of this site are surrounded by negative regions containing minima that are heaped on the positive maximum obstructing its interaction with the negative maxima on the incoming molecules. Therefore, this steric impediment and the very small positive maximum make site 2 unfavorable with respect to site 3 to adsorb molecules similar to PY.

For the Mo edges, the sulfur removal mainly affects the area around the Mo edge and the dark-blue band on the S edge with negative maxima located just at the middle of each of the pairs of the nearest sulfur atoms and is always present for all of the cases (Figure 4g−i). Taking away just one S atom (site 6) produces two five-coordinate Mo atoms on the Mo edge (Figure 4g) by the unit cell. The $V(\mathbf{r})$ mapping (Figure 4g) shows the presence of a cream-yellow region with a maximum of 44.371 kJ/mol at the middle of those five-coordinate Mo atoms. Additional removal of one (site 7) or two (site 8) S atoms creates very acidic sites, located above the four-coordinate Mo atoms with square pyramid geometries, as shown in Figure 4h and i. However, these sites are energetically very unfavorable with respect to site 3. In general, Table 1 and the maps of Figure 4 suggest that the sites that are energetically more favorable are located on the S edges, but their Lewis acid strength is considerably smaller than the site acidity at the Mo edge.

The corresponding $V(\mathbf{r})$ mapping for the $RuS_2$ model is plotted in Figure 5. Yellow- and brown-colored bands of positive $V(\mathbf{r})$ values above the hollow sites with a maximum of 69.576 kJ/mol located just at the middle of each hollow site can be observed. These positive zones are surrounded by negative blue

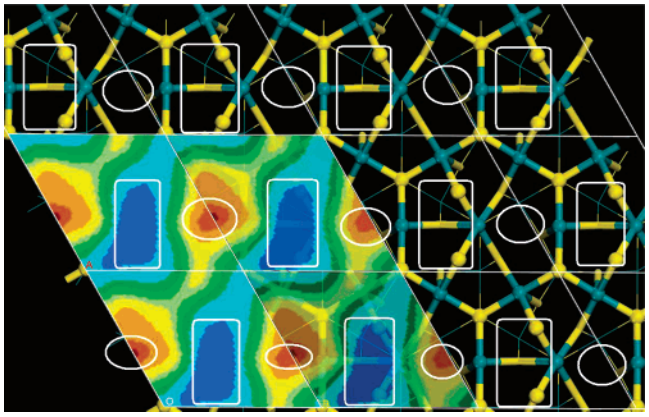

**Figure 5.** Top views of the 0.002 au contour of $\rho(\mathbf{r})$ showing the $V(\mathbf{r})$ mapping onto colors for the $RuS_2(111)$ surface. The color map tab is the same as in Figure 1. White squares and ellipsoids indicate the most negative and positive $V(\mathbf{r})$ zones, respectively. Blue and yellow cylinders denote the Ru and S atoms, respectively. Spheres denote the outermost and exposed atoms of the surface.

bands with a minimum of −51.722 kJ/mol located at the middle of a set of four outermost sulfur atoms bonded to the Ru atoms defining the hollow site. Each of the hollow sites is surrounded by four of those sets of outermost sulfur atoms. Discarding the very unfavorable cases—sites 5 and 8—the suggested trend in Lewis acid strength is

$$\text{site 7} > RuS_2 > \text{site 4} \approx \text{site 3} > \text{site 6} > \text{site 2}$$

To corroborate this trend we studied the adsorption of pyridine on the $RuS_2$ site and sites 7 and 3 of $MoS_2$. Chemisorption of a small basic molecule such as ammonia or pyridine is often used to probe the acidity of solids. We investigated the binding of PY in the $\eta_1$ adsorption configuration (i.e., for the molecule with the ring perpendicular to the surface) on the considered sites, also using DMol[3]. A PY molecule was placed inside the surface 2 × 2 cell, on the considered metal atom site, aligned as the $V(\mathbf{r})$ mapping predicts: the minimum site on the N atom of PY placed over the maximum positive $V(\mathbf{r})$ site on the catalyst's surface. The geometries were fully optimized to their most energetically favorable positions, with the two innermost layers at the bottom of the cell being fixed. The binding energy, BE, was computed as the difference between the total energy of PY adsorbed on the site and the energy of the isolated surface plus the energy of the PY molecule isolated in the cell. The obtained trend for BE was site 7 (142.040 kJ/mol) > $RuS_2$ (126.313 kJ/mol) > site 3 (88.852 kJ/mol). This result confirms the tendency predicted by the $V(\mathbf{r})$-based methodology. Thus, in general, the Lewis acidity for the sites on $RuS_2$ is 100% smaller than for the sites on the Mo edges but around 20% larger than for the most favorable site (site 3) on the S edge of the $MoS_2$. No differences in Lewis acid strength were reported for either catalyst system using FTIR spectroscopy studies[63] with PY as the probe molecule; on Ru and Mo catalysts, pyridine adsorption gives rise to bands (of high intensity) at 1602 and 1600 $cm^{-1}$ (of low intensity), respectively. Therefore, we may conclude that the presence of Lewis acid sites on the Mo edges can be ruled out and that the active site on the $MoS_2$ particles can be the more energetically favorable Lewis acid sites such as site 3 that is located on the S edge. The difference of 20% between the sites on $RuS_2$ and sites such as site 3 could be produced by the presence of the −SH group on the S edge as a consequence of the reduction process using $H_2$. Presently, this aspect is being studied in our laboratory.

## Concluding Remarks

An electrostatic potential-based methodology to locate, visualize, and quantify the strength of Lewis acid sites on surfaces was implemented. The acid strength of sulfur vacancies on the $MoS_2$ edges and the reported most active site on $RuS_2$ was explored using this methodology. The binding of the pyridine molecule on the considered sites has corroborated the trend of Lewis acidity suggested by the electrostatic potential methodology. The obtained results suggest that the presence of Lewis acid sites on the Mo edges can be ruled out and that the active site on the $MoS_2$ particles can be the more energetically favorable sites on the S edges with 50% sulfur coverage.

**Acknowledgment.** This work was supported by grant G-2000001512 from FONACIT (Fondo Nacional de Investigaciones Científicas y Tecnológicas) of Venezuela.

## References and Notes

(1) Weisser, O.; Landa, S. *Sulfide Catalysts: Their Properties and Applications*; Pergamon: Oxford, U.K., 1973.
(2) Topsoe, H.; Clausen, B. S.; Massoth, F. E. *Hydrotreating Catalysis Science and Technology*; Springer-Verlag: Berlin, 1996; Vol. 11.
(3) Rodríguez, J. A.; Drovak, J.; Capitano, A. T.; Gabelnick, A. M.; Gland, J. L. *Surf. Sci.* **1999**, *429*, L462.
(4) Berhault, G.; Lacroix, M.; Breysse, M.; Mauge, F.; Lavalley, J.-C.; Nie, H.; Qu., L. *J. Catal*. **1998**, *178*, 555.
(5) Breysse, M.; Berhault, G.; Kasztelan, S.; Lacroix, M.; Mauge, F.; Perot, G. *Catal. Today* **2001**, *66*, 15.
(6) Diez, R. P.; Jubert, A. H. *J. Mol. Catal*. **1993**, *83*, 219.
(7) Nørskov, J. K.; Clausen, B. S.; Topsøe, H. *Catal. Lett*. **1992**, *13*, 1.
(8) Toulhoat, H.; Kresse, G. *Am. Chem. Soc., Div. Pet. Chem., Prepr*. **1997**, *42*, 114.
(9) Pecoraro, T. A.; Chianelli, R. R. *J. Catal.* **1981**, *67*, 430.
(10) Chianelli, R. R.; Daage, M.; Ledoux, M. J. *Adv. Catal*. **1994**, *40*, 117.
(11) Harris, S.; Chianelli, R. R. *J. Catal.* **1984**, *86*, 400.
(12) Norskov, J. K.; Clausen, B. S.; Topsoe, H. *Catal. Lett.* **1992**, *1*, 13.
(13) Vissers, J. P. R.; Groot, C. K.; van Oers, E. M.; de Beer, V. H. J.; Prins, R. *Bull. Soc. Chim. Belg.* **1984**, *93*, 813.
(14) Ledoux, M. J.; Michaux, O.; Agostini, G.; Panissod, P. *J. Catal*. **1986**, *102*, 275.
(15) Burdett, J. K.; Chung, J. T. *Surf. Sci. Lett.* **1990**, *236*, L353.
(16) Smith, T. S.; Johnson, K. H. *Catal. Lett.* **1994**, *28*, 361.
(17) Raybaud, P.; Kresse, G.; Hafner, J.; Toulhoat, H. *J. Phys.: Condens. Matter* **1997**, *9*, 11085.
(18) Raybaud, P.; Hafner, J.; Kresse, G.; Kasztelan, S.; Toulhoat, H. *J. Catal*. **2000**, *190*, 128.
(19) van Santen, R. A.; Neurock, M. *J. Am. Chem. Soc.* **1994**, *116*, 4427.
(20) Aray, Y.; Rodriguez, J.; Vega, D.; Rodriguez-Arias, E. N. *Angew. Chem., Int. Ed.* **2000**, *39*, 3810.
(21) Clausen, B. S.; Lengeler, B.; Candia, R.; Als-Nielsen, J.; Topsoe, H. *Bull. Soc. Chim. Belg.* **1981**, *90*, 1249.
(22) Parham, T. G.; Merrill, R. P. *J. Catal*. **1984**, *85*, 295.
(23) Tauster, S.; Pecoraro, T.; Chianelli, R. *J. Catal*. **1980**, *63*, 515.
(24) Topsoe, H.; Candia, R.; Topsoe, N. Y.; Clausen, B. S. *Bull. Soc. Chim. Belg.* **1984**, *93*, 783.
(25) Lauritsen, J. V.; Bollinger, M. V.; Laegsgaard, E.; Jacobsen, K. W.; Norskov, J. K.; Clausen, B. S.; Topsoe, H.; Besenbacher, F. *J. Catal.* **2004**, *221*, 510.
(26) Rodríguez, J. A.; Tanhong, C.; Zhen, S.; Hrbek, J. *J. Am. Chem. Soc*. **2004**, *126*, 8886.
(27) Grillo, M. E.; Sautet, P. *J. Mol. Catal. A: Chem*. **2001**, *3195*, 1.
(28) Aray, Y.; Rodríguez, J.; Vega, D.; Coll, S.; Rodríguez-Arias, E.; Rosillo, F. *J. Phys. Chem. B* **2002**, *106*, 13242.
(29) Leboeuf, M.; Koster, M.; Jug, K.; Salahub, D. R. *J. Chem. Phys*. **1999**, *111*, 4893.
(30) Gadre, S. R.; Shirsat, R. N. *Electrostatics of Atoms and Molecules*; Universities Press: Hyderabad, India, 2000.
(31) Pingale, S. S.; Gadre, S. R.; Batolotti, L. J. *J. Phys. Chem. A* **1998**, *102*, 9987. (b) Deshmukh, M. M.; Sastry, N. V., Gadre, S. R. *J. Chem. Phys*. **2004**, *121*, 12402. (c) Joshi, K. A.; Gejji, S. P. *J. Mol. Struct.: THEOCHEM* **2005**, *724*, 87. (d) Tachikawa, H.; Iyama, T.; Kawabata, H. *J. Mol. Struct.: THEOCHEM* **2005**, *718*, 117.
(32) Pathak, R. K.; Gadre, S. R. *J. Chem. Phys.* **1990**, *93*, 1770. (b) Gadre, S. R.; Kulkarni, S. A.; Shrivastava, I. H. *J. Chem. Phys*. **1992**, *96*, 5253.
(33) Gadre, S. R.; Pathak, R. K. *Proc. Indian Acad. Sci., Chem. Sci*. **1989**, *102*, 18.
(34) Alhambra, C.; Luque, F. J.; Orozco, M. *J. Phys. Chem.* **1995**, *99*, 3084. (b) Kornelak, P.; Michalak, A.; Najbar, M. *Catal. Today*. **2005**, *101*, 175. (c) Michalak, A. *Chem. Phys. Lett.* **2004**, *386*, 346.
(35) Politzer, P.; Truhlar, D. G. *Chemical Applications of Atomic and Molecular Electrostatic Potentials*; Plenum: New York, 1982.
(36) Murray, J. S.; Sen, K. D. *Molecular Electrostatic Potential: Concepts and Applications*; Elsevier: Amsterdam, 1996.
(37) Orozco, M.; Luque, F. J. *Theor. Comput. Chem.* **1996**, *3*, 181.
(38) Aray, Y.; Marquez, M.; Rodríguez, J.; Coll, S.; Simón-Manso,Y.; Gonzalez, C.; Weitz, D. A. *J. Phys. Chem. B* **2003**, *107*, 8946.
(39) Aray, Y.; Marquez, M.; Rodríguez, J.; Coll, S.; Simón-Manso, Y.; Gonzalez, C.; Weitz, D. A. *J. Phys. Chem. B* **2004**, *108*, 2418. (b) Aray, Y.; Rodríguez, J.; Coll, S.; Gonzalez, C.; Marquez, M. *J. Phys. Chem. B* **2004**, *108*, 18942.
(40) Tal, Y.; Bader, R. F. W.; Erkku, J. *Phys. Rev. A: At., Mol., Opt. Phys.* **1980**, *21*, 1.
(41) Keith, T. A.; Bader, R. F. W.; Aray, Y. *Int. J. Quantum Chem.* **1996**, *57*, 183.
(42) Sjoberg, P.; Politzer, P. *J. Phys. Chem.* **1990**, *94*, 3959.
(43) Aray, Y.; Rodríguez, J.; Vega, D. *Comput. Phys. Commun*. **2002**, *143*, 199.
(44) Aray, Y.; Rodríguez, J.; Coll, D. S.; González, C.; Márquez, M. *J. Phys. Chem. B* **2004**, *108*, 18942.
(45) *DMol*$^3$ is available as a part of the Material Studio; Accelrys Inc.: San Diego, CA, 2002.
(46) Delley, B. *J. Chem. Phys*. **1990**, *92*, 508. Delley, B. *J. Chem. Phys*. **2000**, *113*, 7756.
(47) Perdew, J. P.; Burke, K.; Emzerhof, M. *Phys. Rev. Lett*. **1996**, *77*, 3865.
(48) Byskov, L. S.; Norskov, J. K.; Clausen, B. S.; Topsoe, H. *Catal. Lett.* **2000**, *64*, 95.
(49) Schweiger, H.; Raybaud, P.; Toulhoat, H. *J. Catal*. **2002**, *212*, 33.
(50) Byskov, L. S.; Norskov, J. K.; Clausen, B. S.; Topsoe, H. *Catal. Lett.* **1997**, *47*, 177.
(51) Byskov, L. S.; Norskov, J. K.; Clausen, B. S.; Topsoe, H. *J. Catal*. **1999**, *187*, 109.
(52) Raybaud, P.; Hafner, J.; Kresse, H.; Toulhoat, H. *Phys. Rev. Lett*. **1998**, *80*, 1481.
(53) Raybaud, P.; Hafner, J.; Kresse, H.; Toulhoat, H. *Surf. Sci.* **1998**, *407*, 237.
(54) Toulhoat, H.; Raybaud, P.; Kasztelan, S.; Kresse, H.; Hafner, J. *Catal. Today* **1999**, 1*87*, 629.
(55) Raybaud, P.; Hafner, J.; Kresse, G.; Kasztelan, S.; Toulhoat, H. *J. Catal*. **2000**, *189*, 129.
(56) Cristol, S.; Paul, J. F.; Payen, E.; Bougeard, D.; Hafner, J.; Hutschka, F. *Stud. Surf. Sci. Catal.* **1999**, *127*, 327.
(57) Cristol, S.; Paul, J. F.; Payen, E.; Bougeard, D.; Clemendot, F.; Hutschka, F. *J. Phys. Chem. B* **2000**, *104*, 11220.
(58) Travert, A.; Nakamura, H.; van Santen, R. A.; Cristol, S.; Payen, E. *J. Am. Chem. Soc.* **2002**, *124*, 7084.
(59) Paul, J. F.; Payen, E. *J. Phys. Chem. B* **2003**, *107*, 4057.
(60) Adjaye, J.; Sun, M.; Nelson, A. *Appl. Catal., A* **2004**, *263*, 131.
(61) Adjaye, J.; Sun, M.; Nelson, A. *J. Catal.* **2004**, *226*, 32.
(62) Lutz, H. D.; Mueller, B.; Schmidt, T.; Sting, T. *Acta Crystallogr., Sect. C* **1990**, *46*, 2003.
(63) Berhault, G.; Lacroix, M.; Breysse, M.; Maugé, F.; Lavalley, J.-C.; Nie, H.; Lianglong, Q. *J. Catal*. **1998**, *178*, 555.